

Analytic Approach for Impact Time Guidance with Look Angle Constraint Using Exact Time-to-Go Solution

Seokwon Lee¹, Jinrae Kim², Youdan Kim³, and Namhoon Cho⁴

ABSTRACT

This paper proposes an analytic approach for impact-control guidance laws against stationary targets using biased proportional navigation. The proposed guidance scheme realizes the impact time control in two different ways: the first approach directly uses the exact time-to-go error to satisfy both the impact-time-control and the field-of-view constraint, while the second approach adopts a look angle tracking law to indirectly control the impact time, with the reference profile of the look angle generated using the exact time-to-go solution. The stability properties of the proposed guidance laws are discussed, and numerical simulations are carried out to evaluate their performance in terms of accuracy and efficiency.

1 INTRODUCTION

Impact time control (ITC) has been a subject of interest in guidance systems for decades. ITC involves completion of the engagement at a specific time, and its importance was initially recognized in anti-ship missile systems for enhancing attack effectiveness and survivability through time-coordination strategies such as salvo attack and sequential strike (Jeon et al. 2010; Zhang et al.

¹Assistant Professor, Department of Mechanical Engineering, Chung-Ang University, Seoul, 06974, Republic of Korea, (corresponding author, e-mail:seokwonlee@cau.ac.kr)

²Ph D Candidate, Department of Aerospace Engineering, Seoul National University, Seoul, 08826, Republic of Korea. (e-mail:kjl950403@snu.ac.kr)

³Professor, Department of Aerospace Engineering, The Institute of Advanced Aerospace Technology, Seoul National University, Seoul, 08826, Republic of Korea. (e-mail:ydkim@snu.ac.kr)

⁴Research Fellow, Centre for Autonomous and Cyber-Physical Systems, School of Aerospace, Transport, and Manufacturing, Cranfield University, Cranfield, MK43 0AL, United Kingdom. (e-mail:n.cho@cranfield.ac.uk)

2020; Tahk et al. 2018; Li and Ding 2018). Moreover, the concept of ITC has been extended to simultaneously consideration of the impact angle (Lee et al. 2007; Harl and Balakrishnan 2012; Kim et al. 2013; Harrison 2012; Livermore and Shima 2018; Hu et al. 2018) and seeker's field-of-view (FOV) limit (Sang and Tahk 2009; Tekin et al. 2016; Zhang et al. 2014; Chen and Wang 2018; Kim and Kim 2019; Erer and Tekin 2016; Jeon and Lee 2017; Tekin et al. 2017a; Tekin et al. 2017b; Tekin and Erer 2020; Kim et al. 2020; Saleem and Ratnoo 2016; Wang et al. 2019; Tsalik and Shima 2019; Lee et al. 2020; Dong et al. 2022; Kang et al. 2023a).

Recent research has considered the seeker's field-of-view (FOV) limit in the design of ITC. The FOV limit restricts the missile's maneuverability to maintain its look angle within a predefined FOV consistently. Studies on ITC with a look angle constraint can be broadly classified into two categories. The first category involves directly handling the impact time error in terms of time-to-go while ensuring the look angle constraint is met. Biased proportional navigation guidance (BPNG) have been widely adopted to regulate the impact time error by means of ITC (Sang and Tahk 2009; Tekin et al. 2016; Lee et al. 2020; Zhang et al. 2014; Kim et al. 2021; Cho and Lee 2021; He et al. 2020). Sang and Tahk (Sang and Tahk 2009) proposed a switching framework to cope with the FOV constraint, while Tekin et al. (Tekin et al. 2016) analyzed the range of achievable time with respect to the FOV constraint. Zhang et al. (Zhang et al. 2014) proposed an impact-time-control guidance law using BPNG and an approximate model to generate the impact time error. He et al. (He et al. 2020) designed the impact-time control guidance (ITCG) via optimal error feedback formulation.

The second category involves designing the ITCG using an indirect controlled variable in terms of look angle error, rather than time-to-go error. Two approaches have been employed in this category: trajectory shaping guidance and reference-tracking type guidance (Jeon and Lee 2017; Tekin et al. 2017a; Tekin et al. 2017b; Tekin et al. 2018; Tekin and Erer 2020; Kim et al. 2020; Kim et al. 2021). In the trajectory shaping approach, the guidance law is designed by shaping the trajectory to satisfy multiple constraints expressed as polynomials of variables such as range and look angle. The terminal time and FOV constraints are satisfied by appropriately

45 selecting the coefficients of the polynomials, and the guidance command is generated to follow the
46 trajectory profile. In general, the trajectory shaping methods include online optimization process
47 to select the coefficients. For impact time control problem, total path length and FOV limit are
48 imposed as equality and inequality constraints, respectively. The parameter selection process is
49 then formulated as a parametric optimization problem, which may require additional computation.
50 In the reference-tracking type approach, a reference is designed to satisfy boundary conditions
51 such as impact time and look angle constraints. An error feedback routine is then incorporated to
52 control the variable and follow the reference. While these approaches offer advantages in shaping
53 the guidance trajectory while satisfying the constraints, they essentially follow an open-loop control
54 procedure and are sensitive to performance errors due to uncertainties.

55 In both approaches, accurate time-to-go information is crucial for achieving ITC and ensur-
56 ing precise timing coordination and control. The time-to-go information is used to measure the
57 remaining time and impact time error and is incorporated directly or indirectly in the ITC. How-
58 ever, obtaining the time-to-go information through nonlinear control schemes (Kim et al. 2015;
59 Kumar and Ghose 2015; Cho et al. 2016; Kim et al. 2019a; Hu et al. 2019) can be challenging, as
60 closed-loop kinematics must be solved exactly. Some research works modified the PNG by varying
61 the navigation gain, which leads to obtain solvable closed-loop kinematics and reduce computa-
62 tional burden (Dong et al. 2023; Kang et al. 2023b). On the other hand, ITC schemes based on
63 proportional navigation guidance (PNG) (Jeon et al. 2006; Cho and Kim 2016) have been found
64 useful in obtaining the time-to-go solution, as the guided trajectory can be obtained in closed form.
65 Nevertheless, the accuracy of existing methods for time-to-go calculation is limited by the use of
66 approximate solutions (Tahk et al. 2018; Ryoo et al. 2006; Dhananjay and Ghose 2014), which
67 can degrade performance in explicit time-to-go guidance laws. In both direct and indirect impact
68 time control approaches, guidance laws are often designed using linearized engagement kinematics
69 (Jeon et al. 2006) or approximate time-to-go forms (Zhang et al. 2014; He et al. 2020), leading to
70 unsatisfactory performance due to inaccuracies in the relationship between time-to-go and control
71 variables.

72 This study presents an analytic approach to design guidance laws for ITC, where an exact
73 time-to-go solution is derived for precise impact time error. Motivated by the previous studies
74 (Cho and Kim 2016; Kim et al. 2021), the study designs BPNG laws that satisfy the look angle
75 constraint while maintaining PNG performance. A pure proportional navigation guidance (PPNG)
76 serves as a baseline guidance law, and the exact time-to-go solution is used to accurately track
77 ITC. The study introduces an additional bias input to compensate for the impact time error, and
78 various error variables can be chosen to design the bias command. The proposed guidance laws are
79 suitable for two ITCG approaches: explicit time-to-go error regulation and feedback law synthesis,
80 and control of impact time through the tracking of the reference look angle profile. Lyapunov
81 stability theory is used to investigate error convergence and positive invariance of the look angle
82 solution. The study also includes discussions on guidance law design guidelines, and similarities
83 and comparisons between the proposed guidance laws.

84 This study makes several contributions. Firstly, the proposed analytic approach utilizes exact
85 time-to-go solutions, resulting in more accurate impact time control compared to existing methods
86 that rely on approximate time-to-go formulas. The use of analytic solutions enables designers to
87 effectively analyze the guidance laws and significantly improve performance, particularly near the
88 interception moment. Secondly, the proposed methods are designed using the BPNG framework,
89 which preserves the benefits of the BPNG technique. The BPNG approach handles impact time
90 error and look angle constraints using a bias input, while the PNG is used for intercept capability
91 during the terminal phase. Both proposed guidance laws comply with the BPNG structure and
92 utilize its features. Thirdly, the proposed guidance laws generate continuous inputs, resulting in
93 more stable performance than the existing two-stage guidance laws (Sang and Tahk 2009; Lee
94 et al. 2020). Finally, comparative discussion provides insight into possible variations of the BPNG
95 design for ITCG.

96 **2 PROBLEM FORMULATION AND PRELIMINARIES**

97 In this section, the equations of motion for the missile and target are described in Sec. 2.1. The
98 guidance objective considered in this study is then described in Sec. 2.2.

2.1 Equations of Motion

Consider the planar motion of a missile with respect to a stationary target as shown in Fig. 1. The following assumptions are used throughout this study.

Assumption 1. The interceptor is considered as a lag-free vehicle maintaining a constant speed.

Assumption 2. The angle of attack is negligible.

The look angle is defined as

$$\sigma = \gamma - \lambda \quad (1)$$

where γ is the flight-path angle of the missile. λ is the line-of-sight (LOS) angle, respectively.

Under Assumption 2, the engagement kinematics can be expressed in polar coordinates as

$$\dot{r} = -V_m \cos \sigma \quad (2a)$$

$$r\dot{\lambda} = -V_m \sin \sigma \quad (2b)$$

$$\dot{\gamma} = \frac{a_m}{V_m} \quad (2c)$$

where r is the distance between the missile and the target. V_m is the speed of the missile. a_m represents the acceleration perpendicular to the velocity vector.

Using Eq. (2) in (1), we have

$$\dot{\sigma} = \frac{V_m}{r} \sin \sigma + \frac{a_m}{V_m} \quad (3)$$

2.2 Problem Definition for impact-time-control

In this section, the problem considered in this study is described according to the design goals. First, this study focuses on the guidance law for target interception at a desired impact time. For instance, the interception must be performed with zero miss distance at the desired impact time. The miss distance in terms of zero-effort-miss can be considered as

$$Z = r \sin \sigma \quad (4)$$

121 The zero-effort-miss is nullified if σ or r regulate before interception. Note that r strictly decreases
 122 if the look angle satisfies

$$123 \quad \dot{r} = -V_m \cos \sigma < 0 \quad \text{for} \quad |\sigma| < \frac{\pi}{2} \quad (5)$$

124 Otherwise, the unbounded look angle response increases range and also diverges the guidance
 125 command. It is also desirable to regulate the acceleration command in the vicinity of the interception
 126 considering the energy-minimization point of view. Note that LOS rate should be zero for stationary
 127 target interception. To satisfy both requirements, the terminal condition of σ can be expressed as

$$128 \quad \dot{\lambda} = -\frac{V_m}{r} \sin \sigma \rightarrow 0 \text{ as } r \rightarrow 0 \quad \Rightarrow \quad \sigma \rightarrow 0 \text{ as } r \rightarrow 0 \quad (6)$$

129 Meanwhile, the look angle should remain consistently within the FOV. The look angle constraint
 130 can be expressed as follows:

$$131 \quad \sigma(t) \in \Sigma = [-\sigma_{\text{lim}}, \sigma_{\text{lim}}], \quad \forall t \in [t_0, t_f] \quad (7)$$

132 where σ_{lim} is bounded from above by $\pi/2$. The look angle constraint can be achieved if Σ is a
 133 positively invariant set and $\sigma(t_0) \in \Sigma$ (Khalil, H. K., and Grizzle 1996). Note that r decreases
 134 with respect to time, i.e., Eq.(5), as long as the missile maintains its target inside the seeker's
 135 field-of-view for all time, as represented in Eq. (7). In summary, the impact-time-control problem
 136 can be stated as follows:

- 137 1) (Terminal Condition) The range and the look angle at the impact time must be regulated,
 138 i.e., $r \rightarrow 0$ and $\sigma \rightarrow 0$.
- 139 2) (Positive Invariance of Σ , Eq. (7)) The set Σ should be positively invariant. That is,
 140 $\sigma(t_0) \in \Sigma \Rightarrow \sigma(t) \in \Sigma, \forall t_0 \leq t \leq t_f$.
- 141 3) (Desired Impact Time) The impact-time error should be less than the allowed value, i.e.,
 142 $|t_f - t_d| \leq \epsilon$, where t_d is a desired impact time.

143 3 ANALYTIC APPROACH FOR TIME-TO-GO SOLUTION

144 This section outlines the exact solution of the time-to-go that will be used for designing ITCG
 145 laws. The proposed guidance scheme employs the PPNG as the baseline guidance performance.
 146 The fundamental characteristics of PPNG are briefly summarized in Section 3.1. Section 3.2
 147 presents the derivation of the time-to-go solution, which is based on the closed-form solution of
 148 PPNG.

149 **3.1 Pure Proportional Navigation**

150 The basic principle of the PNG is to steer the vehicle to form a stable collision geometry with
 151 the guidance command that is proportional to the LOS rate. In this study, PPNG is considered as a
 152 baseline guidance command. The PPNG command is given by (Zarchan 2012)

$$153 \quad a_{PPNG} = NV_m \dot{\lambda} = -N \frac{V_m^2}{r} \sin \sigma \quad (8)$$

154 where N is the navigation gain. Using the lateral acceleration generated by the PPNG, i.e.,
 155 $a_m = a_{PPNG}$, the differential relations of the flight-path angle and look angle can be obtained to be
 156 proportional to the LOS angle as

$$157 \quad \dot{\gamma} = N \dot{\lambda} \quad (9a)$$

$$158 \quad \dot{\sigma} = \dot{\gamma} - \dot{\lambda} = (N - 1) \dot{\lambda} \quad (9b)$$

159 Using Eqs. (2a), (2b) and (9b), σ and λ can be evolved with respect to r as

$$160 \quad \sin \sigma = \sin \sigma_0 \left(\frac{r}{r_0} \right)^{N-1} \quad (10)$$

$$161 \quad \lambda = -\frac{V_m \sin \sigma_0}{r_0} \left(\frac{r}{r_0} \right)^{N-2} \quad (11)$$

163 From Eqs. (10) and (11), the permissible navigation constant satisfying the terminal condition can
 164 be expressed as follows: (Shneydor 1998; Zarchan 2012)

- 165 1. $\sigma(r_f = 0) = 0$ if and only if $N > 1$

166 2. $\dot{\lambda}(r_f = 0) = 0$ if and only if $N > 2$

167 3.2 Analytic Solution for Time-to-go

168 The analytic solution for the time-to-go of the PPNG was derived when the target is stationary
 169 (Cho and Kim 2016) and is expressed as a function of N , V_m , r and σ as

$$170 t_{go,PPN}(r, \sigma; N) = \frac{r}{V_m} \mathcal{F}(|\sigma|; N) \quad (12)$$

171 where $\mathcal{F}(|\sigma|; N)$ is defined as

$$172 \mathcal{F}(|\sigma|; N) \triangleq \begin{cases} {}_2\mathcal{F}_1\left(\frac{1}{2}, \frac{1}{2(N-1)}; 1 + \frac{1}{2(N-1)}; \sin^2 \sigma\right) & |\sigma| \leq \frac{\pi}{2} \\ \frac{2}{|\sin \sigma|^{1/N-1}} {}_2\mathcal{F}_1\left(\frac{1}{2}, \frac{1}{2(N-1)}; 1 + \frac{1}{2(N-1)}; 1\right) - {}_2\mathcal{F}_1\left(\frac{1}{2}, \frac{1}{2(N-1)}; 1 + \frac{1}{2(N-1)}; \sin^2 \sigma\right) & \frac{\pi}{2} < |\sigma| < \pi \end{cases} \quad (13)$$

173 The function ${}_2\mathcal{F}_1\left(\frac{1}{2}, \frac{1}{2(N-1)}; 1 + \frac{1}{2(N-1)}; \sin^2 \sigma\right)$ can also be expressed as an infinite series:

$$174 {}_2\mathcal{F}_1\left(\frac{1}{2}, \frac{1}{2(N-1)}; 1 + \frac{1}{2(N-1)}; \sin^2 \sigma\right) = \sum_{n=0}^{\infty} \frac{(2n)!}{2^{2n} (1 + 2n(N-1)) (n!)^2} |\sin \sigma|^{2n} \quad (14)$$

175 where ${}_2\mathcal{F}_1(a, b; c; z)$ is a Gaussian hyper-geometric function (GHGF) defined as in (Gasper et al.
 176 2004). Note that GHGF is an even function with respect to σ . Because of its symmetricity, the
 177 GHGF $\mathcal{F}(|\sigma|; N)$ satisfies

$$178 \mathcal{F}(|\sigma|; N) \geq 1, \quad \forall |\sigma| \in [0, \pi), \quad \text{and} \quad \mathcal{F}(0, N) = 1 \quad (15)$$

179 For the derivation of the partial derivatives, the GHGF for $c = b + 1$ is given by (Cho and Kim
 180 2016; Gasper et al. 2004; Kim et al. 2021)

$$181 \frac{\partial {}_2\mathcal{F}_1(a, b, b+1; z)}{\partial z} = \frac{b}{z} ((1-z)^{-a} - {}_2\mathcal{F}_1(a, b, b+1; z)) \quad (16)$$

182 Using the above property, the partial derivative of \mathcal{F} can be obtained as

$$183 \quad \frac{\partial \mathcal{F}(|\sigma|; N)}{\partial |\sigma|} = \frac{|\cot \sigma|}{N-1} (\sec \sigma - \mathcal{F}(|\sigma|; N)), \quad \forall \sigma \in (0, \pi) \quad (17)$$

184 Accordingly, the partial derivative of the time-to-go, $t_{go,PPN}$, given by (12) can be represented
185 as

$$186 \quad \frac{\partial t_{go,PPN}}{\partial r} = \frac{\mathcal{F}(|\sigma|; N)}{V_m} = \frac{t_{go,PPN}}{r} \quad (18)$$

$$187 \quad \frac{\partial t_{go,PPN}}{\partial |\sigma|} = \frac{r}{V_m} \frac{|\cot \sigma|}{N-1} \left(\sec \sigma - \frac{V_m}{r} t_{go,PPN} \right) = \frac{1}{N-1} \frac{(t_{go,DPP} - t_{go,PPN})}{|\tan \sigma|} \quad (19)$$

188 where $t_{go,DPP}$ represents the time-to-go of the deviated pure pursuit guidance law (Lee et al. 2020)
189 that can be represented as

$$190 \quad t_{go,DPP} = \frac{r}{V_m \cos \sigma} \quad (20)$$

191 Since $t_{go,DPP} - t_{go,PPN} > 0$ for all $\sigma \in \Sigma \setminus \{0\}$, the following properties hold for the partial
192 derivative.
193

$$194 \quad \frac{1}{\cos \sigma} > \mathcal{F}(\sigma; N), \quad \text{or} \quad 1 - \cos \sigma \mathcal{F}(\sigma; N) > 0 \quad (21a)$$

$$195 \quad \frac{\partial t_{go,PPN}}{\partial |\sigma|} \propto \frac{\partial \mathcal{F}(|\sigma|; N)}{\partial |\sigma|} > 0, \quad \forall |\sigma| \in (0, \pi) \quad (21b)$$

$$196 \quad \lim_{\sigma \rightarrow 0} \frac{\partial t_{go,PPN}}{\partial |\sigma|} = \frac{r}{V_m} \lim_{\sigma \rightarrow 0} \frac{\partial \mathcal{F}(|\sigma|; N)}{\partial |\sigma|} = 0 \quad (21c)$$

197 where backlash operator \setminus indicates the relative complement between sets defined by $A \setminus B = \{x | x \in$
198 $A, x \notin B\}$ Later, the above properties will be utilized in the ITCG design.

199 **Remark 1.** (Approximate Solution of PPNG Time-to-Go) The exact solution of $t_{go,PPNG}$ can be
200 expressed as an infinite series of $\sin^2 \sigma$, and it is possible to approximate the solution by taking the
201 first few terms of the series expansion. For example, expansion of the series up to the first order in

202 $\sin^2 \sigma$ gives an approximate expression for the time-to-go as

$$203 \quad t_{go,approx} \approx \frac{r}{V_m} \sum_{n=0}^1 \frac{(2n)!}{2^{2n}(1+2n(N-1))(n!)^2} |\sin \sigma|^{2n} = \frac{r}{V_m} \left(1 + \frac{\sin^2 \sigma}{2(2N-1)} \right) \quad (22)$$

204 Under small angle assumption, $\sin \sigma \approx \sigma$, it can be further approximated as

$$205 \quad t_{go,approx,small} \approx \frac{r}{V_m} \left(1 + \frac{\sigma^2}{2(2N-1)} \right) \quad (23)$$

206 Approximate expressions for the time-to-go were used to design guidance laws for the impact-time-
207 control in Refs. (Zhang et al. 2014; He et al. 2020).

208 **Remark 2.** (Implementation of the GHGF) The implementation of the exact time-to-go requires
209 calculating the GHGF or the incomplete beta function. Several methods have been developed to
210 ensure efficient and accurate computation, including: i) solving the related differential equation, ii)
211 reading from a table, and iii) using hybrid calculation methods based on the range of input (Pearson
212 2009). These methods have already been incorporated into numerous software packages designed
213 for implementing special functions (Lozier 2003).

214 The effectiveness of implementation method was discussed with comparison of time-to-go
215 computation methods (Cho and Kim 2016). It can be observed that the evaluation of the partial sum
216 approximation is slow, and the results are inaccurate. In contrast, the calculation of time-to-go using
217 GHGF or the incomplete beta function show good accuracy without sacrificing computational time.
218 This is because computing a function is faster and more advantageous than iteratively summing a
219 series.

220 4 PROPOSED GUIDANCE LAWS

221 This section presents ITCG laws to achieve interception at the desired impact time while
222 preserving the characteristics of PPNG. The guidance laws follow BPNG structure consisting of
223 the PPNG as the baseline guidance and the bias input for the regulation of impact time error. The

224 guidance command can be represented as

$$225 \quad a_m = a_{PPN} + a_{bias} = -N \frac{V_m^2}{r} \sin \sigma + a_{bias} \quad (24)$$

226 where a_{bias} is the biased term to be designed. Substitution of Eq. (24) into Eq. (3) yields the
227 differential equation of σ as

$$228 \quad \dot{\sigma} = -(N - 1) \frac{V_m}{r} \sin \sigma + \frac{a_{bias}}{V_m} \quad (25)$$

229 Note that it is possible to design a_{bias} in various ways for the impact-time-control. In this study,
230 two approaches for bias input design are proposed based on the exact time-to-go of the baseline
231 trajectory. In Sec. 4.1, a time-to-go error feedback law is designed using the exact time-to-go
232 solution of the PPNG. In Sec. 4.2, a look-angle control guidance law is proposed for impact-time-
233 control considering the look angle constraint. The characteristics of the proposed guidance laws
234 are discussed in Sec. 4.3.

235 **4.1 Guidance Law 1: Direct impact-time-control Based on Exact Time-to-Go**

236 In this section, an ITCG law is designed using the explicit feedback of impact time error. Let
237 us define the time-to-go error as

$$238 \quad e_t = t_{go,PPN} - t_{go}^d \quad (26)$$

239 where $t_{go}^d = t_d - t$ is the desired time-to-go.

240 The desired time-to-go should be chosen within the feasible region, otherwise the guidance
241 objectives cannot be achieved simultaneously. Considering the physical constraints, one may select
242 the feasible region $\Gamma \in (\frac{r}{V_m}, \frac{r}{V_m \cos \sigma_{lim}})$ for the desired time-to-go (Lee et al. 2020).

243 First, let us design the bias input for stabilizing the error variable defined in Eq. (26). For this,
244 taking the time derivative of e_t along the closed-loop trajectory by the guidance command, Eq.

245 (24), and substituting Eqs. (2), (18)-(20), and (25), into the resulting equation yields

$$\begin{aligned}
\dot{e}_t &= \dot{t}_{go,PPN} - (-1) = \frac{\partial t_{go,PPN}}{\partial r} \dot{r} + \frac{\partial t_{go,PPN}}{\partial |\sigma|} \dot{\sigma} \operatorname{sgn}(\sigma) + 1 \\
&= \frac{t_{go,PPN}}{r} (-V_m \cos \sigma) + 1 + \frac{1}{N-1} \frac{t_{go,DPP} - t_{go,PPN}}{\tan |\sigma|} \left(-(N-1) \frac{V_m}{r} \sin \sigma + \frac{a_{bias}}{V_m} \right) \operatorname{sgn}(\sigma) \\
&= \frac{1}{(N-1)V_m} \frac{t_{go,DPP} - t_{go,PPN}}{\tan \sigma} a_{bias} \\
&\triangleq B_t(\sigma) a_{bias}
\end{aligned}
\tag{27}$$

246 where $\operatorname{sgn}(x)$ is defined as

$$\operatorname{sgn}(x) = \begin{cases} 1 & x > 0 \\ 0 & x = 0 \\ -1 & x < 0 \end{cases}
\tag{28}$$

249 The error dynamics of Eq. (27) are linear in a_{bias} . According to Eqs. (19) and (21), if the absolute
250 value of the look angle is bounded as $|\sigma| > \underline{\sigma} > 0$, then B_t is also bounded as

$$|B_t(\sigma)| \geq \frac{1}{V_m} \left. \frac{\partial t_{go,PPN}}{\partial \sigma} \right|_{\sigma=\underline{\sigma}} > 0
\tag{29}$$

252 The bias input should be properly designed to stabilize the error dynamics while satisfying the
253 look angle constraint. For this, let us propose the bias input a_{bias} as

$$a_{bias,1} = -(N-1) \frac{V_m^2}{r} \sin \sigma_{lim} (\operatorname{sgn}(\sigma) f(\sigma)) \operatorname{sgn}(e_t) \left(\frac{|e_t|}{|e_t(0)|} \right)^\alpha
\tag{30}$$

255 where $0 < \alpha \leq 1$ is a positive parameter introduced for finite-time convergence.

256 Note that $\alpha = 1$ represents the linear error feedback with state-dependent varying gain and
257 $f(\sigma)$ is a smooth shaping function satisfying the following conditions (Kim et al. 2019b; Kim et al.
258 2021)

$$\begin{aligned}
f(\sigma) &\geq 1 \quad \text{if } \sigma \in \Sigma \\
f(\sigma) &= 1 \quad \text{if } \sigma = \pm \sigma_{lim}
\end{aligned}
\tag{31}$$

260 The shaping function is required for preserving the positive invariance of the set Σ . One may
 261 choose the shaping function from various functions satisfying the boundary conditions. The error
 262 dynamics associated with the bias input $a_{bias,1}$ can be expressed by using Eq. (30) in Eq. (27) as

$$\begin{aligned}
 \dot{e}_t &= B_t(\sigma)a_{bias,1} = \frac{1}{(N-1)V_m} \frac{t_{go,DPP} - t_{go,PPN}}{\tan \sigma} a_{bias,1} \\
 &= -V_m \sin \sigma_{lim} \left(\frac{t_{go,DPP} - t_{go,PPN}}{\tan \sigma} \right) \frac{1}{r} \frac{\sigma}{|\sigma|} f(\sigma) \text{sgn}(e_t) \left(\frac{|e_t|}{|e_t(0)|} \right)^\alpha \\
 &= -V_m \sin \sigma_{lim} \left(\frac{t_{go,DPP} - t_{go,PPN}}{|\tan \sigma|} \right) \frac{1}{r} f(\sigma) \text{sgn}(e_t) \left(\frac{|e_t|}{|e_t(0)|} \right)^\alpha
 \end{aligned} \tag{32}$$

264 For stability analysis, let us consider the following Lyapunov candidate function.

$$V_1 = \frac{1}{2} e_t^2 \tag{33}$$

266 The time derivative of V_1 along the error dynamics given by Eq. (32) can be obtained substituting
 267 Eq. (19) as

$$\begin{aligned}
 \dot{V}_1 &= \dot{e}_t e_t = -V_m \sin \sigma_{lim} \left(\frac{t_{go,DPP} - t_{go,PPN}}{|\tan \sigma|} \right) \frac{f(\sigma)}{r} \frac{|e_t|^{1+\alpha}}{|e_t(0)|^\alpha} \\
 &= -(N-1)V_m \sin \sigma_{lim} \left(\frac{\partial t_{go,PPN}}{\partial |\sigma|} \right) \frac{f(\sigma)}{r} \frac{(2V_1)^{\frac{1+\alpha}{2}}}{|e_t(0)|^\alpha} \leq 0
 \end{aligned} \tag{34}$$

269 Note that $N > 2$. According to Eq. (21), V_1 monotonically decreases as long as $\sigma \neq 0$. To
 270 demonstrate the finite-time convergence of the error e_t , the Lyapunov function is further expanded
 271 by using Eqs. (2), (9), (12), (17) (19), (20) and (30) into Eq. (34) as

$$\begin{aligned}
 \dot{V}_1 &= (N-1) \sin \sigma_{lim} \left(\frac{\partial t_{go,PPN}}{\partial |\sigma|} \right) \frac{-V_m \cos \sigma}{r \cos \sigma} \frac{f(\sigma)}{|e_t(0)|^\alpha} (2V_1)^{\frac{1+\alpha}{2}} \\
 &= (N-1) \sin \sigma_{lim} \left(\frac{\partial t_{go,PPN}}{\partial |\sigma|} \right) \frac{\dot{r}}{r \cos \sigma} \frac{f(\sigma)}{|e_t(0)|^\alpha} (2V_1)^{\frac{1+\alpha}{2}} \\
 &\leq \frac{2^{\frac{1+\alpha}{2}} \sin \sigma_{lim}}{|e_t(0)|^\alpha} V_1^{\frac{1+\alpha}{2}} \left(\frac{t_{go,DPP} - t_{go,PPN}}{|\tan \sigma|} \right) \frac{\dot{r}}{r} = \frac{2^{\frac{1+\alpha}{2}} \sin \sigma_{lim}}{V_m |e_t(0)|^\alpha} V_1^{\frac{1+\alpha}{2}} \left(\frac{\sec \sigma - \mathcal{F}(|\sigma|; N)}{|\tan \sigma|} \right) \dot{r} \\
 &= \frac{2^{\frac{1+\alpha}{2}} (N-1) \sin \sigma_{lim}}{V_m |e_t(0)|^\alpha} V_1^{\frac{1+\alpha}{2}} \left(\frac{\partial \mathcal{F}(|\sigma|; N)}{\partial |\sigma|} \right) \dot{r}
 \end{aligned} \tag{35}$$

273 It is desired to regulate the time-to-go error before $(r, \sigma) \rightarrow (0, 0)$ to recover the performance of

274 the baseline guidance. Let $r_1 > 0$ be a required distance at which the time-to-go error vanishes,
 275 and σ_1 is the corresponding look angle. The stability of the time-to-go error dynamics leads to
 276 $\sigma \in [\underline{\sigma}, \bar{\sigma}] \subset \Sigma / \{0\}$ and $\frac{\partial \mathcal{F}}{\partial \sigma} \Big|_{\underline{\sigma}} \leq \frac{\partial \mathcal{F}}{\partial \sigma}$. Equation (35) can be rewritten as

$$277 \quad \frac{dV_1}{V_1^{\left(\frac{1+\alpha}{2}\right)}} \leq C_1 dr \quad (36)$$

278 where $C_1 = \frac{2^{\frac{1+\alpha}{2}}(N-1) \sin \sigma_{\text{lim}}}{V_m |e_t(0)|^\alpha} \frac{\partial \mathcal{F}}{\partial \sigma} \Big|_{\underline{\sigma}}$.

279 Integrating both sides of Eq. (36) gives

$$280 \quad \frac{2}{1-\alpha} \left((V_1(r))^{\left(\frac{1-\alpha}{2}\right)} - (V_1(0))^{\left(\frac{1-\alpha}{2}\right)} \right) \leq C_1 (r - r_0) \quad (37)$$

281 Considering the boundary condition $V_1(r_1) = 0$, the settling distance r_1 is bounded from below as
 282 described by

$$283 \quad r_1 \geq r_{1,\min} = r_0 - \frac{2}{C_1(1-\alpha)} V_1(0)^{\frac{1-\alpha}{2}} = r_0 - \frac{V_m}{(N-1)(1-\alpha) \sin \sigma_{\text{lim}} \frac{\partial \mathcal{F}}{\partial \sigma} \Big|_{\underline{\sigma}}} |e_t(0)| \quad (38)$$

284 From Eq. (38), smaller α and $|e_t(0)|$ result in larger $r_{1,\min}$, contributing to faster time-to-go error
 285 convergence.

286 Considering the seeker's FOV limit, the proposed guidance law should ensure the positive
 287 invariance of Σ . To investigate this property, let us rewrite the σ -dynamics as

$$288 \quad \dot{\sigma} = -(N-1) \frac{V_m}{r} \left(\sin \sigma + \sin \sigma_{\text{lim}} f(\sigma) \frac{\sigma}{|\sigma|} \text{sgn}(e_t) \left(\frac{|e_t|}{|e_t(0)|} \right)^\alpha \right) \quad (39)$$

289 Consider the storage function V_σ defined as

$$290 \quad V_\sigma(\sigma) = \frac{1}{2} (\sin \sigma)^2 \quad (40)$$

291 Note that the set $M = \{\sigma(t) : V_\sigma(|\sigma(t)|) \leq V_\sigma(\sigma_{\text{lim}}), \quad \forall t \in [t_0, t_f]\}$ is equivalent to Σ . Therefore,

292 using the Lyapunov stability theory, the positively invariant set Σ can be proved by showing that
 293 the M is a positively invariant level set. By differentiating Eq. (40) with respect to time, and using
 294 Eq. (39) in the resulting equation, we obtain the time derivative of the storage function evaluated
 295 at the boundary as

$$296 \quad \dot{V}_\sigma(\pm\sigma_{\text{lim}}) = -(N-1)\frac{V_m}{r} \cos \sigma_{\text{lim}} \sin^2 \sigma_{\text{lim}} \left(1 + f(\sigma_{\text{lim}}) \text{sgn}(e_t) \left(\frac{|e_t|}{|e_t(0)|} \right)^\alpha \right) < 0 \quad (41)$$

297 Note that the terms inside the bracket of Eq. (41) is greater than zero because of the boundary
 298 condition of $f(\sigma_{\text{lim}}) = 1$. Therefore, M is a positively invariant set, and so is Σ .

299 **4.2 Guidance Law 2: Indirect impact-time-control via Look-Angle Control**

300 This section presents an indirect approach to design an ITCG by controlling the look angle
 301 (Kim et al. 2021). Suppose that the desired impact time is achieved by the baseline guidance law,
 302 i.e., PPNG. Then, the desired look angle associated with the desired impact time can be determined
 303 by

$$304 \quad t_{go}^d = t_{go,PPN}^d(r, |\sigma_d|; N) = \frac{r}{V_m} \mathcal{F}(|\sigma_d|; N) \quad (42)$$

305 There exists a one-to-one correspondence between $|\sigma|$ and $t_{go,PPN}$, and therefore the desired
 306 value $|\sigma_d|$ can be obtained by the inverse mapping of Eq. (42) as

$$307 \quad |\sigma_d| = \mathcal{F}^{-1}\left(\frac{V_m}{r} t_{go,PPN}^d; N\right) \quad (43)$$

308 Note that the inverse mapping cannot be analytically obtained because the inverse of the GHGF
 309 $\mathcal{F}(|\sigma|; N)$ is not available. Since $\mathcal{F}(|\sigma|; N)$ is monotonically increasing on the interval $|\sigma| \in$
 310 $[0, \sigma_{\text{lim}}]$, $|\sigma_d|$ can be easily obtained by numerical methods developed for line search or root finding.
 311 To resolve the sign ambiguity of σ , σ_d can be determined using the current sign of the current look
 312 angle as follows:

$$313 \quad \sigma_d = |\sigma_d| \text{sgn}(\sigma) \quad (44)$$

314 The desired look angle σ_d varies with elapsed time. The time derivative can be obtained by

315 differentiating Eq. (42) with respect to time and using Eqs. (2), (17)-(19) in the resulting equation
 316 as

$$-1 = \frac{\partial t_{go,PPN}}{\partial r} \dot{r} + \frac{\partial t_{go,PPN}}{\partial |\sigma_d|} \dot{\sigma}_d \text{sgn}(\sigma_d) = \frac{t_{go,PPN}}{r} (-V_m \cos \sigma) + \frac{\cot \sigma_d}{N-1} (t_{go,DPP} - t_{go,PPN}) \dot{\sigma}_d \quad (45)$$

317 where $t_{go,PPN}$ and $t_{go,DPP}$ in Eq. (45) are the values obtained from the desired look angle σ_d .

318 Using Eqs. (12) and (19), Eq. (45) can be rewritten with respect to $\dot{\sigma}_d$ as

$$\begin{aligned} \dot{\sigma}_d &= -(N-1) \frac{V_m}{r} \left(\frac{r}{V_m} - \cos \sigma t_{go,PPN} \right) \frac{\tan \sigma_d}{t_{go,DPP} - t_{go,PPN}} \\ &= -(N-1) \frac{V_m}{r} \frac{1 - \cos \sigma \mathcal{F}(\sigma_d; N)}{1 - \cos \sigma_d \mathcal{F}(\sigma_d; N)} \sin \sigma_d \end{aligned} \quad (46)$$

320 where $\mathcal{F}(\sigma_d; N)$ can be calculated from Eq. (13).

321 Note that there is a symmetric relation between the time-to-go and the look angle, and the look
 322 angle is within the symmetric bound, i.e., $-\sigma_{\text{lim}} \leq \sigma \leq \sigma_{\text{lim}}$. Without a loss of generality, let us
 323 consider the positive look angle case $\sigma > 0$ and $\sigma_d > 0$.

324 For guidance law design, let us define the error variable e_σ for the impact-time-control as

$$e_\sigma = \sigma - \sigma_d \quad (47)$$

325 Taking time derivative of Eq. (47) and using Eqs. (25) and (46) in the resultant equation, the error
 326 dynamics of e_σ can be obtained as

$$\begin{aligned} \dot{e}_\sigma &= -(N-1) \frac{V_m}{r} \sin \sigma + (N-1) \frac{V_m}{r} \frac{1 - \cos \sigma \mathcal{F}(\sigma_d; N)}{1 - \cos \sigma_d \mathcal{F}(\sigma_d; N)} \sin \sigma_d + \frac{a_{bias}}{V_m} \\ &\triangleq (F_\sigma(\sigma, r) - \dot{\sigma}_d(\sigma, \sigma_d, r)) + \frac{1}{V_m} a_{bias} \end{aligned} \quad (48)$$

327 where

$$F_\sigma(\sigma, r) = -(N-1) \frac{V_m}{r} \sin \sigma \quad (49)$$

328 Considering the guidance objectives stated in Sec. 2.2, the look angle σ should remain in Σ for

333 all time. For this, let us propose the bias input as

$$334 \quad a_{bias,2} = -V_m (F_\sigma(\sigma, r) - \dot{\sigma}_d) - (N - 1) \frac{V_m^2}{r} \cos \sigma (k f(\sigma)) \operatorname{sgn}(e_\sigma) \left(\frac{|e_\sigma|}{|e_\sigma(0)|} \right)^\alpha \quad (50)$$

335 where $k > 0$ is a design parameter, and $f(\sigma)$ is the shaping function defined as same as in Sec.
336 4.1.

337 The first term of $a_{bias,2}$ cancels out the nonlinear effect of the error dynamics, and the second
338 term is a feedback term to achieve the finite-time convergence of e_σ as well as the positive invariance
339 of Σ . The error dynamics of e_σ associated with the biased input can be expressed as

$$340 \quad \dot{e}_\sigma = -(N - 1) \frac{V_m}{r} \cos \sigma k f(\sigma) \operatorname{sgn}(e_\sigma) \left(\frac{|e_\sigma|}{|e_\sigma(0)|} \right)^\alpha \quad (51)$$

341 To verify the stability of the proposed guidance law, let us introduce the following Lyapunov
342 candidate function.

$$343 \quad V_2 = \frac{1}{2} e_\sigma^2 \quad (52)$$

344 Differentiating Eq. (52) with respect to time, and substituting Eq. (50) into the resulting equation
345 yields the time derivative of V_2 along the error dynamics of e_σ as

$$346 \quad \dot{V}_2 = -(N - 1) \frac{V_m \cos \sigma}{r} k f(\sigma) \frac{|e_\sigma|^{1+\alpha}}{|e_\sigma(0)|^\alpha} < 0 \quad (53)$$

347 Equation (53) shows that \dot{V}_2 is negative definite becomes $N > 2$ and $f(\sigma) \geq 1$, and therefore the
348 equilibrium point $e_\sigma = 0$ is asymptotically stable.

349 Now, let us demonstrate the finite-time convergence of the error variable. Substituting Eqs. (2),
350 (52), and the condition $f(\sigma) \geq 1$ into Eq. (53) gives

$$351 \quad \frac{\dot{V}_2}{V_2^{\frac{1+\alpha}{2}}} \leq (N - 1) \frac{2^{\frac{1+\alpha}{2}}}{|e_\sigma(0)|^\alpha} \frac{\dot{r}}{r} k \quad (54)$$

352

$$V_2^{-\frac{1+\alpha}{2}} dV_2 \leq C_2 k \frac{1}{r} dr \quad (55)$$

353

354 where $C_2 = (N - 1) \frac{2^{\frac{1+\alpha}{2}}}{|e_{\sigma}(0)|^{\alpha}}$.

355 Integrating each side of Eq. (55) gives

$$\frac{2}{1 - \alpha} \left(V_2(r)^{\frac{1-\alpha}{2}} - V_2(r_0)^{\frac{1-\alpha}{2}} \right) \leq k C_2 \ln \left(\frac{r}{r_0} \right) \quad (56)$$

356

357 Considering the boundary condition for the finite-time convergence, i.e., $V_2(r) = 0$, $r \geq r_{s2}$, the
 358 settling distance r_{s2} can be bounded from below as

$$\begin{aligned} r_{s2} &\geq r_{s2,\min} := r_0 \exp \left(\frac{-2}{(1 - \alpha) k (N - 1) \frac{2^{\frac{1+\alpha}{2}}}{|e_{\sigma}(0)|^{\alpha}}} V_2(r_0)^{\frac{1-\alpha}{2}} \right) \\ &= r_0 \exp \left(- \frac{|e_{\sigma}(0)|}{(1 - \alpha) k (N - 1)} \right) \end{aligned} \quad (57)$$

359

360 During the maneuver, σ should be kept consistently in Σ . If the desired value is consistently
 361 in the invariant set Σ , convergence of e_{σ} to zero along the dynamics of Eq. (51) automatically
 362 ensures the positive invariance of Σ . That is, $\sigma_d \in \Sigma \forall t \in [t_0, t_f] \Rightarrow \sigma \in \Sigma$ as $\sigma \rightarrow \sigma_d$. In this
 363 respect, let us consider the case that the desired look angle is initially set beyond the limited value,
 364 i.e., $\sigma_{d0} > \sigma_{\lim}$. Then, the time derivative of the look angle satisfies

$$\begin{aligned} \dot{\sigma}_d(\sigma, \sigma_d, r) \sigma &= -(N - 1) \frac{V_m}{r} \left(\frac{1 - \cos \sigma \mathcal{F}(\sigma_d; N)}{1 - \cos \sigma_d \mathcal{F}(\sigma_d; N)} \right) \sin \sigma_d \sigma < 0 \\ &\text{if } \cos^{-1} \left(\frac{1}{\mathcal{F}(\sigma_d; N)} \right) \leq |\sigma| \leq \sigma_{\lim} \end{aligned} \quad (58)$$

365

366 Figure 2 shows the typical profiles of the desired look angle. If the initial look angle satisfies
 367 $\sigma_0 < \cos^{-1} \left(\frac{1}{\mathcal{F}(\sigma_{d0}; N)} \right) < \sigma_{\lim} < \sigma_{d0}$, the desired look angle increases with increasing look angle
 368 to regulate the error. Then, the desired look angle reaches the maximum value at which the desired
 369 value σ_d^* and the instant look angle σ^* satisfy $\mathcal{F}(\sigma_d^*; N) = \frac{1}{\cos \sigma^*}$. Then, the desired look angle
 370 monotonically decreases, $\sigma_d^* > \sigma_d$. On the other hand, if the initial look angle and the desired

371 value initially satisfy $\cos^{-1}\left(\frac{1}{\mathcal{F}(\sigma_{d0}; N)}\right) < \sigma_0 < \sigma_{\text{lim}} < \sigma_{d0}$, then the desired value monotonically
 372 decreases from the initial phase. To ensure the error regulation while maintaining the look angle
 373 constraint, the guidance gain k should be properly determined. From Eqs. (45), (46) and (50), the
 374 time derivative of σ at the boundary can be expressed as

$$\begin{aligned} \dot{\sigma}|_{\sigma=\sigma_{\text{lim}}} &= \dot{\sigma}_d - (N-1)\frac{V_m}{r} \cos \sigma_{\text{lim}} k f(\sigma_{\text{lim}}) \text{sgn}(e_\sigma) \left(\frac{|e_\sigma|}{|e_\sigma(0)|}\right)^\alpha \\ &= -(N-1)\frac{V_m}{r} \left(\frac{1 - \cos \sigma_{\text{lim}} \mathcal{F}(\sigma_d; N)}{1 - \cos \sigma_d \mathcal{F}(\sigma_d; N)}\right) \sin \sigma_d + \cos \sigma_{\text{lim}} k f(\sigma) \text{sgn}(e_\sigma) \left(\frac{|e_\sigma|}{|e_\sigma(0)|}\right)^\alpha \end{aligned} \quad (59)$$

375
 376 Note that $f(\sigma_{\text{lim}}) = 1$. For the storage function V_σ defined in Eq. (40), \dot{V}_σ at the boundary $\sigma = \sigma_{\text{lim}}$
 377 can be obtained as

$$\begin{aligned} \dot{V}_\sigma(\sigma_{\text{lim}}) &= \cos \sigma_{\text{lim}} \sin \sigma_{\text{lim}} \dot{\sigma}|_{\sigma=\sigma_{\text{lim}}} = -(N-1)\frac{V_m}{r} \cos \sigma_{\text{lim}} \sin \sigma_{\text{lim}} \\ &\quad \left(\frac{1 - \cos \sigma_{\text{lim}} \mathcal{F}(\sigma_d; N)}{1 - \cos \sigma_d \mathcal{F}(\sigma_d; N)} \sin \sigma_d + \cos \sigma_{\text{lim}} k \text{sgn}(e_\sigma) \left(\frac{|e_\sigma|}{|e_\sigma(0)|}\right)^\alpha\right) \end{aligned} \quad (60)$$

379 At the boundary $\sigma = \sigma_{\text{lim}}$, the following inequalities hold

$$1 > \frac{1 - \cos \sigma_{\text{lim}} \mathcal{F}(\sigma_d; N)}{1 - \cos \sigma_d \mathcal{F}(\sigma_d; N)} \geq \frac{1 - \cos \sigma_{\text{lim}} \mathcal{F}(\sigma_d^*; N)}{1 - \cos \sigma_d^* \mathcal{F}(\sigma_d^*; N)} =: \underline{\Delta} > 0 \quad (61a)$$

$$\sin \sigma_d \sin \sigma_{\text{lim}} > \sin^2 \sigma_{\text{lim}} \quad (61b)$$

382 Using the above inequalities, the upper bound of the design parameter can be determined as

$$k < \tan \sigma_{\text{lim}} \underline{\Delta} \quad (62)$$

384 Then, \dot{V}_σ is bounded above zero as

$$\dot{V}_\sigma(\sigma_{\text{lim}}) \leq -(N-1)\frac{V_m}{r} \cos \sigma_{\text{lim}} \underline{\Delta} \sin^2 \sigma_{\text{lim}} \left(1 + \frac{k}{\underline{\Delta} \tan \sigma_{\text{lim}}} \text{sgn}(e_\sigma) \left(\frac{|e_\sigma|}{|e_\sigma(0)|}\right)^\alpha\right) < 0 \quad (63)$$

386 In summary, the design parameter k should be bounded by $0 < k \leq \tan \sigma_{\text{lim}} \underline{\Delta}$. The lower

387 bound is made for error tracking, and the upper bound ensures that the look angle will not to exceed
388 the FOV limit while tracking the desired look angle, respectively.

389 **Remark 3.** (Prevention of singularity of biased command when $t_{go} \in \left(\frac{r}{\sqrt{v_m}}, t_{go,PPN}\right)$) The desired
390 time-to-go can be smaller than the predicted time-to-go for the PPNG. In that case, it should be
391 guaranteed that the lead angle profile does not maintain zero in a finite interval. One way to avoid
392 the singularity is to reset the navigation gain N depending on the desired impact time. If the impact
393 time is smaller than the PPNG for the current gain set, $t_{go}^d < t_{go,PPN}$, then N can be increased to
394 reduce the current t_{go} so that $t_{go,PPN}(N_{new}) < t_{go}^d$. Afterwards, the biased term will contribute to
395 elongating the flight path in order to achieve the desired impact time.

396 4.3 Discussions of Proposed Guidance Laws

397 *Behaviors of Guidance Laws and Guidelines for Design Parameter Selection*

398 In this section, let us discuss how the proposed guidance laws behave from the perspective of
399 BPNG. In the initial period of the terminal phase, two guidance components, a_{PPNG} and a_{bias}
400 consistently steer the missile heading to enter a collision course for desired impact time. In this
401 period, the effect of the bias input is dominant in the guidance command. The time-to-go error
402 indicates the predicted intercept time error when the baseline guidance is only in action. The
403 correction of the impact time error implies that the initial condition is being adjusted to the proper
404 one to finish the PPNG at the desired impact time. Once the error dynamics are stabilized, then the
405 guidance command becomes equivalent to PPNG. The time-to-go is obtained based on the PPNG,
406 and therefore the error correction can be performed by complying with the performance of the
407 baseline guidance. As a whole, the stabilization of the error dynamics plays the most important
408 role in this framework. This study employs the finite-time convergent error dynamics that appear
409 in many pieces of literature on sliding mode control scheme (Shtessel et al. 2007; Levant 2001;
410 Zhang et al. 2014). Three kinds of design parameters contribute to stabilizing the error dynamics.
411 The properties of the parameters on the performance of the guidance laws are discussed as follows.

- 412 • (Exponent of the error, α) : α attributes to the nonlinear error feedback and leads to finite-

time convergence of the error dynamics. The lower α improves the convergent rate of the error dynamics but rapidly drives the error to be regulated and causes a non-uniform response when the error is close to zero. To prevent this issue, it is recommended to choose α carefully and properly.

- (Shaping function, $f(\sigma)$) : $f(\sigma)$ generally acts as the varying gain in terms of σ that shapes the trajectory, which also ensures that the look angle remains within the limit value. Considering the boundary condition (31), one may choose an even and concave function with different basis. For example, if the smooth "hat-shaped" function is considered, which is mostly flat over the interval $\sigma \in (-\sigma_{\text{lim}} + \epsilon, \sigma_{\text{lim}} - \epsilon)$ for a small constant ϵ and changes to 1 rapidly at $\sigma = \pm\sigma_{\text{lim}}$, then the maneuver abruptly changes to keep look angle within the limit value. As the extreme case, $\epsilon \rightarrow 0$, the shaping function is made a discontinuous form, and the response becomes similar to two-stage guidance approach (Sang and Tahk 2009; Tekin et al. 2017a; Lee et al. 2020). This maneuver may take advantages of the look angle keeping and yield a large achievable impact time set (Tekin et al. 2017a; Lee et al. 2020) but also brings an abrupt guidance command.
- (Proportional Feedback in the second approach, k) : k mainly amplifies the effect of the error terms in the bias input. A large k increases the convergent rate of the error response, but it should be bounded by Eq. (62) for the consideration of look angle limit. One possible way to select k is to consider the linearized formulation as Eq. (68).

Comparison with Inaccurate Time-to-go

This section examines how the exact solution improves the impact time control compared to the approximate one. Aforementioned in Remark 1, the impact time error e_t can be expressed in terms of the approximate solution as

$$e_t = t_{go,PPN} - t_{go}^d = t_{go,approx} + \Delta_t - t_{go}^d = e_{t,approx} + \Delta_t \quad (64)$$

437 where Δ_t is the time-to-go between the exact solution and the approximate one. Note that Δ_t
 438 consists of higher-order terms expressed as r and σ , which vary with respect to time. For brevity,
 439 it is assumed that $|\Delta_t| \leq b_1$ and $|\dot{\Delta}_t| \leq b_2$ for small positive b_1 and b_2 . Suppose that guidance
 440 laws based on the approximate time-to-go solution are properly designed so that the closed-loop
 441 dynamics become Hurwitz as $\dot{e}_{t,approx} = -K_1 e_{t,approx}$. Then, the true error dynamics e_t can be
 442 obtained as

$$443 \quad \dot{e}_t = -K_1 e_{t,approx} + K_1 \Delta_t + \dot{\Delta}_t \quad (65)$$

444 Therefore, the residual error $\Delta \triangleq K_1 \Delta_t + \dot{\Delta}_t$ prevents the error from converging to zero unless it is
 445 suppressed. Note also that even the small impact time error induces the fast diverging response to
 446 the LOS rate and causes large miss distance. On the other hand, the proposed guidance laws utilize
 447 the exact time-to-go and fully account for the true impact time error. Therefore, the residual error
 448 is compensated, which improves the impact time precision and decreases the miss distance.

449 *Comparison Between Proposed Guidance Laws*

450 The proposed guidance laws using both approaches comply with BPNG structure and exhibit
 451 common characteristics discussed in Sec. 4.3. This section addresses the comparison between the
 452 proposed guidance laws in regard to similarities and distinct properties. First, let us examine the
 453 differences in the commands. The main differences between the guidance laws presented in Secs.
 454 4.1 and 4.2 are as follows: i) controlled variables (e_t, e_σ), and ii) design parameters ($f(\sigma), k$). Let
 455 us consider an approximate time-to-go under the small angle assumption, Eq. (23). Assuming that
 456 σ_d is obtained from the approximate solution, the impact time error can be approximated using the
 457 Taylor series expansion as

$$458 \quad \begin{aligned} e_t &\approx \hat{t}_{go,PPN} - \hat{t}_{go,PPN}^d = \frac{r}{V_m} \left(1 + \frac{\sigma^2}{2(2N-1)} \right) - \frac{r}{V_m} \left(1 + \frac{\sigma_d^2}{2(2N-1)} \right) \\ &= \frac{r}{2(2N-1)V_m} (\sigma^2 - \sigma_d^2) \end{aligned} \quad (66)$$

459 The bias input $a_{bias,1}$ in the guidance law 1, Eq. (30), for $\alpha = 1$ can be rewritten as

$$\begin{aligned}
 a_{bias,1} &= -(N-1)V_m^2 \frac{\sin \sigma_{lim}}{r} [sgn(\sigma)f(\sigma)] \left(\frac{e_t}{|e_t(0)|} \right) \\
 &\approx -(N-1)V_m^2 \frac{\sin \sigma_{lim}}{r_0} [sgn(\sigma)f(\sigma)] \frac{\sigma^2 - \sigma_d^2}{|\sigma_0^2 - \sigma_{d,0}^2|}
 \end{aligned} \tag{67}$$

461 Considering Eq. (67), the design parameter k can be chosen to express the guidance law 2, Eq.
 462 (50), in a form similar to the guidance law 1. The particular k can be chosen as

$$k = sgn(\sigma) \frac{\sigma + \sigma_d}{|\sigma_0 + \sigma_{d,0}|} \frac{r}{r_0} (\tan \sigma_{lim}) \underline{\Delta} \leq \tan \sigma_{lim} \underline{\Delta} \tag{68}$$

464 Setting $\alpha = 1$, the bias input $a_{bias,2}$ in the guidance law 2 can be rewritten as

$$\begin{aligned}
 a_{bias,2} &= -V_m (F_\sigma(\sigma, r) - \dot{\sigma}_d) - (N-1) \frac{V_m^2}{r_0} \sin \sigma_{lim} sgn(\sigma) \left(\frac{\cos \sigma}{\cos \sigma_{lim}} \right) \underline{\Delta} f(\sigma) \frac{\sigma^2 - \sigma_d^2}{|\sigma_0^2 - \sigma_{d,0}^2|} \\
 &= -V_m (F_\sigma(\sigma, r) - \dot{\sigma}_d) + \frac{\cos \sigma}{\cos \sigma_{lim}} \underline{\Delta} a_{bias,1}
 \end{aligned} \tag{69}$$

466 It can be observed from the approximated guidance laws that their similarities arise from the
 467 feedback action. In the guidance law 2, $a_{bias,2}$, the feedback part is roughly proportional to $a_{bias,1}$,
 468 but $a_{bias,2}$ also contains nonlinear cancellation terms, as shown in Eq. (69). The feedback action
 469 is reduced as the look angle approaches the limited value.

$$\frac{\cos \sigma}{\cos \sigma_{lim}} \underline{\Delta} |a_{bias,1}| \approx \underline{\Delta} |a_{bias,1}| \ll |a_{bias,1}|, \quad \text{as } \sigma \rightarrow \sigma_{lim} \tag{70}$$

471 Meanwhile, one can also differentiate the proposed guidance laws using two approaches from
 472 one another. In the first approach, the guidance law utilizes the impact time error based on exact
 473 time-to-go. In this aspect, it can be regarded that the direct control of the impact time error is a more
 474 intuitive way to deal with the impact time control. The guidance law could also be much robust
 475 if the measurement error is involved in practice. On the other hand, in the second approach, the
 476 reference profile can be modified for trajectory shaping in addition to selecting design parameters.

477 As shown in Fig. 2, the look angle constraint can be incorporated into the design of the look angle
 478 reference. The look angle reference σ_r can be defined not to exceed the FOV limit as described by

$$479 \quad \sigma_r = \text{sgn}(\sigma_d) \min(|\sigma_d|, \sigma_{\text{lim}}) \quad (71)$$

480 The guidance law considering the reference profile can be designed to regulate the look angle error
 481 between σ and σ_r as

$$482 \quad a_{\text{bias},2a} = -V_m \left((F_\sigma(\sigma_r, r) - \varphi(e_\sigma, \sigma) \dot{\sigma}_d) + K(r, \sigma) \frac{\sigma - \sigma_r}{|e_\sigma(0)|} \right) \quad (72)$$

483 where $K(r, \sigma) > 0$ is the positive gain function for a feedback action. In Eq. (72), $\varphi(e_\sigma, \sigma)$ is an
 484 activation function defined as follows

$$485 \quad \varphi(e_\sigma, \sigma) = \begin{cases} 1 & \text{if } \dot{\sigma}_d e_\sigma < 0 \\ 0 & \text{if } \dot{\sigma}_d e_\sigma \geq 0 \end{cases} \quad (73)$$

486 Note that the desired look angle σ_d is replaced by σ_r in Eq. (72). Through these processes,
 487 the similarity between the reference tracking law and two-stage guidance laws (Lee et al. 2020)
 488 can be shown. Assume that the look angle reference is generated considering the limit value
 489 $\sigma_0 \leq \sigma_{\text{lim}} < \sigma_d$. Then, the bias reference allows the look angle to follow the limit value. After the
 490 look angle converges to the reference $\sigma_r = \pm\sigma_{\text{lim}}$ at the instant t_1 , the trajectory by the proposed
 491 guidance law is equivalent to that presented in (Lee et al. 2020). After σ converges to σ_r , the
 492 profile of σ can be obtained as (Lee et al. 2020)

$$493 \quad \sigma(t) = \begin{cases} \sigma_{\text{lim}}, & r_{sw} \leq r \leq r_1 \\ \sin^{-1} \left(\sin \sigma_{\text{lim}} \left(\frac{r}{r_{sw}} \right)^{N-1} \right), & 0 \leq r \leq r_{sw} \end{cases} \quad (74)$$

494 where r_{sw} is the transition range that can be calculated as

$$495 \quad r_{sw} = V_m \frac{\frac{r_1}{V_m \cos \sigma_{lim}} - (t^d - t_1)}{\sec \sigma_{lim} - \mathcal{F}(\sigma_{lim}; N)} \quad (75)$$

496 The maintaining the limit value continues until σ_r changes to σ_d . After σ_r transition, the look
 497 angle error is regulated. Then, the resultant guidance law is governed by the PPNG. In this fashion,
 498 the second approach using the reference, $a_{bias,2a}$, would produce wider set of the achievable impact
 499 time than the first approach. In comparison to the two-stage guidance law (Lee et al. 2020), the
 500 feedback action of the proposed method makes the guidance system more robust against the initial
 501 heading error and model uncertainty.

502 **5 NUMERICAL SIMULATION**

503 Numerical simulations were conducted to evaluate the performance of the proposed guidance
 504 laws in three different scenarios. In all simulation cases, the initial distance between the missile
 505 and target was set to 10,000 m, the missile speed was set to 300 m/s, and the initial look angle was
 506 30° . The missile's maximum acceleration was set to 300 m/s^2 , and the FOV limit was set to 60° .
 507 A navigation constant of $N = 3$ was chosen, and the simulation step size was set to 500 Hz. Other
 508 parameters were scenario-dependent. The simulations were terminated when the relative distance
 509 r between the missile and target was less than 0.3.

510 **5.1 Scenario 1: Performance Effects of Design Parameters**

511 In the first scenario, the bias input $a_{bias,1}$ is considered among the three proposed guidance laws,
 512 and the effect of the design parameters $f(\sigma)$ and α on the performance of the proposed guidance
 513 law 1 is investigated. As discussed in Sec. 4.3, the shaping function $f(\sigma)$ and the exponent α will
 514 affect the performance, and the following shaping functions are considered.

$$515 \quad f_1(\sigma) = \left(\frac{\cos \sigma}{\cos \sigma_{lim}} \right)^p, \quad f_2(\sigma) = 1 + a \left(1 - \left(\frac{|\sigma|}{\sigma_{lim}} \right)^b \right) \quad (76)$$

516 where $(p, a, b) = (6, 63, 5)$ are chosen. Table 1 summarizes the simulation cases considered in this
 517 scenario.

518 Figure 3 shows the simulation results of the first scenario. To achieve the desired impact time,
 519 the missile steers to increase the look angle. As the look angle approaches the FOV limit, the
 520 guidance law enables the look angle not to exceed the FOV limit. As shown in Fig. 3e, the smooth
 521 and continuous response is observed in the guidance command while achieving the look angle
 522 constraint and impact time, which is advantageous over multi-stage type guidance laws (Lee et al.
 523 2020). The shaping function exerts substantial influences on the performance as it adjusts the
 524 trend of the trajectory. In comparison to the case using f_1 , the look angle approaches closer to the
 525 boundary and stays near the boundary for a longer period of time when f_2 is used. As shown in
 526 Fig. 3d, the graph of the function f_2 is flat around the origin and changes sharply near the FOV
 527 limit. The flattened shaping function creates a tendency for the look angle to be maintained near
 528 the look angle boundary. Meanwhile, it is observed that a smaller α reduces regulation time as
 529 shown in Fig. 3c. It can be concluded that the shaping function mainly affects the initial phase of
 530 the flight while the exponent α influences the regulation time. It is also found that the performance
 531 is sensitive to the change of α when f_1 is used as the shaping function, which indicates that the
 532 design parameters should be selected in pairs.

533 **5.2 Scenario 2: Comparison with Guidance Laws Based on Approximate Time-to-Go**

534 In the second scenario, the effect of the time-to-go accuracy on the ITCG is evaluated. The
 535 missile is required to intercept the target at $t_d = 55$ seconds while maintaining the look angle within
 536 the FOV limit, $\sigma_{\text{lim}} = 60$ deg. For comparison, guidance laws based on approximate time-to-go
 537 is considered that are summarized in Table 2. To exclude the sources of trajectory variation other
 538 than the time-to-go relation used in the comparative study, the guidance commands in Refs. (Zhang
 539 et al. 2014) and (He et al. 2020) are modified so that the error dynamics follow the following form
 540 that is similar to Eq. (32).

$$541 \quad \dot{e}_t + K_e \text{sgn}(e_t) \left(\frac{|e_t|}{|e_t(0)|} \right)^\alpha = 0 \quad (77)$$

542 Figure 4 shows the simulation results of the scenario 2. The missile is required to increase the
543 flight time to achieve the desired impact time, and therefore, the look angle increases until it reaches
544 the limit value. As shown in Figs. 4d- 4b, all guidance laws regulate the time-to-go error while
545 the look angle remained within the FOV. To satisfy the look angle constraint, each guidance law
546 exhibits slightly different behavior, which can be attributed to the different shaping functions. Note
547 that the proposed guidance law uses f_1 as the shaping function, Eq. (76), which is less flat. The
548 shaping function f_1 leads the look angle of the proposed guidance scheme to keep decreasing after it
549 reaches its maximum value as shown in Fig. 4b. The shaping function used in Ref. (He et al. 2020)
550 makes the look angle stay near the FOV for a longer period of time, which is advantageous for faster
551 convergence of the impact time error as compared to other schemes. After the time-to-go error
552 vanishes, the baseline guidance law, PPNG, allows the missile to complete the flight. However, it
553 is observed that the guidance commands using the approximated formulae become divergent near
554 the interception. It is clear that the approximate time-to-go cannot be perfectly compensated for
555 the effect of the approximation error due to the truncation and small angle assumption. Although
556 the time-to-go error defined with respect to an approximate expression for the time-to-go vanishes,
557 the actual time-to-go may still be nonzero, leading to potential instabilities near the end of the
558 engagement.

559 **5.3 Scenario 3: Comparison Between Proposed Guidance Laws**

560 In the last scenario, the performance of the proposed guidance laws are compared. In this
561 simulation, the missile autopilot dynamics is considered as a first-order lag system with a time
562 constant $\tau = 0.1$ s. Two different values are considered for the desired impact time, i.e., $t_d = 45$
563 and 50 seconds. Table 4 summarizes the simulation cases for scenario 3. For a fair comparison,
564 design parameters for the guidance laws $a_{bias,2}$ and $a_{bias,2a}$ are chosen in accordance with Eq.
565 (68). For quantitative comparison of the proposed guidance laws, an average energy consumption
566 is considered as the performance index.

$$567 \quad J_{energy} = \frac{1}{t_f} \int_{t_0}^{t_f} a_m^2(t) dt, \quad (78)$$

568 Figure 5 shows the simulation results for the scenario 3. The proposed guidance laws generate
569 smooth guidance commands to achieve the look angle constraint and impact time as shown in
570 Fig. 5e. Despite the time-lag response induced by the autopilot, the proposed guidance laws show
571 satisfactory performance for the impact time and miss distance. The feedback routine based on
572 the exact time-to-go in the proposed guidance laws provide improved robust performance against
573 autopilot delay compared to the existing open-loop type methods. It is shown that the guidance
574 laws $a_{bias,1}$ and $a_{bias,2}$ present similar responses as discussed in Sec. 4.3. Compared to the
575 guidance law 1, the missile using $a_{bias,2}$ maintains the look angle near the limit for a longer time,
576 because the feedback command for the look angle is reduced when approaching its limit value. It is
577 also observed that the reference modification in the second method, using $a_{bias,2a}$ shows different
578 response compared to two guidance laws. The look angle profile tracks the limit value until the
579 time-to-go error vanishes, and the guidance command shows a relatively abrupt transition after the
580 error regulation, which is similar to two-stage guidance laws (Lee et al. 2020). This behavior leads
581 to stable interception near collision and would produce much wider range of achievable impact
582 time. Table 4 summarizes the simulation results. The proposed guidance methods achieve precise
583 impact time and small miss distance. Relatively, the guidance law 1 shows accurate impact time
584 precision, and guidance law 2a is effective judged by overall performance measures J_{energy} , miss
585 distance, and time-to-go error.

586 6 CONCLUSION

587 This study proposed new biased proportional navigation guidance laws via analytic approach for
588 impact-time-control under look angle constraints. The proposed guidance laws utilized the exact
589 time-to-go solution of the proportional navigation guidance to maintain the performance advantages
590 of the baseline guidance law near the end of engagement. The proposed guidance schemes
591 based on both direct and indirect control of the time-to-go error achieved satisfactory impact time
592 performance while also satisfying the look angle constraint. Furthermore, the proposed schemes
593 demonstrated higher accuracy in impact-time-control compared to existing methods that rely on
594 approximate time-to-go expressions. Overall, the proposed guidance laws provide a promising

595 approach to achieve precise impact-time-control under look angle constraints, which can be further
596 extended to cooperative guidance problem of multiple missiles.

597 **DATA AVAILABILITY STATEMENT**

598 Some or all data, models, or code that support the findings of this study are available from the
599 corresponding author upon reasonable request.

600 **ACKNOWLEDGMENTS**

601 This work was supported by the Chung-Ang University Research Grants in 2023 and the
602 National Research Foundation of Korea(NRF) grant funded by the Korea government(MSIT) (No.
603 RS-2023-00251551).

604 **REFERENCES**

- 605 Chen, X. and Wang, J. (2018). “Nonsingular Sliding-Mode Control for Field-of-View Constrained
606 Impact Time Guidance.” *Journal of Guidance, Control, and Dynamics*, 41(5), 1210–1218.
- 607 Cho, D., Kim, H. J., and Tahk, M. J. (2016). “Nonsingular Sliding Mode Guidance for Impact Time
608 Control.” *Journal of Guidance, Control, and Dynamics*, 39(1), 61–68.
- 609 Cho, N. and Kim, Y. (2016). “Modified Pure Proportional Navigation Guidance Law for Impact
610 Time Control.” *Journal of Guidance, Control, and Dynamics*, 39(4), 852–872.
- 611 Cho, N. and Lee, S. (2021). “Look-angle-constrained control of arrival time with exact knowledge
612 of time-to-go.” *Journal of Guidance, Control, and Dynamics*, 44(10), 1902–1908.
- 613 Dhananjay, N. and Ghose, D. (2014). “Accurate Time-to-Go Estimation for Proportional Navigation
614 Guidance.” *Journal of Guidance, Control, and Dynamics*, 37(4), 1378–1383.
- 615 Dong, W., Wang, C., Wang, J., Son, H., and Xin, M. (2022). “Unified method for field-of-view-
616 limited homing guidance.” *Journal of Guidance, Control, and Dynamics*, 45(8), 1415–1434.
- 617 Dong, W., Wang, C., Wang, J., and Xin, M. (2023). “Varying-gain proportional navigation guidance
618 for precise impact time control.” *Journal of Guidance, Control, and Dynamics*, 46(3), 535–552.
- 619 Erer, K. S. and Tekin, R. (2016). “Impact Time and Angle Control Based on Constrained Optimal
620 Solutions.” *Journal of Guidance, Control, and Dynamics*, 39(10), 2445–2451.

621 Gasper, G., Rahman, M., and George, G. (2004). *Basic Hypergeometric Series*, Vol. 96. Cambridge
622 University Press, Cambridge, UK.

623 Harl, N. and Balakrishnan, S. N. (2012). “Impact Time and Angle Guidance with Sliding Mode
624 Control.” *IEEE Transactions on Control Systems Technology*, 20(6), 1436–1449.

625 Harrison, G. A. (2012). “Hybrid Guidance Law for Approach Angle and Time-of-Arrival Control.”
626 *Journal of Guidance, Control, and Dynamics*, 35(4), 1104–1114.

627 He, S., Lee, C.-H., Shin, H.-S., and Tsourdos, A. (2020). *Optimal Guidance and Its Applications*
628 *in Missiles and UAVs*. Springer, Gewerbestr, Switzerland.

629 Hu, Q., Han, T., and Xin, M. (2018). “New Impact Time and Angle Guidance Strategy via Virtual
630 Target Approach.” *Journal of Guidance, Control, and Dynamics*, 41(8), 1755–1765.

631 Hu, Q., Han, T., and Xin, M. (2019). “Sliding-mode impact time guidance law design for various
632 target motions.” *Journal of Guidance, Control, and Dynamics*, 42(1), 136–148.

633 Jeon, I. S. and Lee, J. I. (2017). “Impact-Time-Control Guidance Law with Constraints on Seeker
634 Look Angle.” *IEEE Transactions on Aerospace and Electronic Systems*, 53(5), 2621–2627.

635 Jeon, I. S., Lee, J. I., and Tahk, M. J. (2006). “Impact-Time-Control Guidance Law for Anti-Ship
636 Missiles.” *IEEE Transactions on Control Systems Technology*, 14(2), 260–266.

637 Jeon, I. S., Lee, J. I., and Tahk, M. J. (2010). “Homing Guidance Law for Cooperative Attack of
638 Multiple Missiles.” *Journal of Guidance, Control, and Dynamics*, 33(1), 275–280.

639 Kang, H., Wang, P., and Song, S. (2023a). “A generalized three-dimensional cooperative
640 guidance law for various communication topologies with field-of-view constraint.” *Proceed-*
641 *ings of the Institution of Mechanical Engineers, Part G: Journal of Aerospace Engineering*,
642 09544100231153265.

643 Kang, H., Wang, P., Wei, S., and Song, S. (2023b). “Three-dimensional impact-time-constrained
644 proportional navigation guidance using range-varying gain.” *Aerospace Science and Technology*,
645 108419.

646 Khalil, H. K., and Grizzle, J. W. (1996). *Nonlinear Systems*, Vol. 3. Prentice hall, Upper Saddle
647 River, NJ.

648 Kim, H. G., Cho, D., and Kim, H. J. (2019a). “Sliding Mode Guidance Law for Impact Time Con-
649 trol without Explicit Time-to-go Estimation.” *IEEE Transactions on Aerospace and Electronic*
650 *Systems*, 55(1), 236–250.

651 Kim, H. G. and Kim, H. J. (2019). “Backstepping-based Impact Time Control Guidance Law for
652 Missiles with Reduced Seeker Field-of-View.” *IEEE Transactions on Aerospace and Electronic*
653 *Systems*, 55(1), 82–94.

654 Kim, H.-G., Lee, J.-Y., Kim, H. J., Kwon, H.-H., and Park, J.-S. (2020). “Look-Angle-Shaping
655 Guidance Law for Impact Angle and Time Control with Field-of-View Constraint.” *IEEE Trans-*
656 *actions on Aerospace and Electronic Systems*, 56(2), 1602–1612.

657 Kim, J., Cho, N., and Kim, Y. (2019b). “Field-of-view constrained impact angle control guidance
658 guaranteeing error convergence before interception.” *AIAA Scitech 2019 Forum*, 1927.

659 Kim, J., Cho, N., and Kim, Y. (2021). “Field-of-view-constrained impact angle control guidance
660 with error convergence before interception considering speed changes.” *Proceedings of the*
661 *Institution of Mechanical Engineers, Part G: Journal of Aerospace Engineering*, 235(2), 238–
662 256.

663 Kim, M., Jung, B., Han, B., Lee, S., and Kim, Y. (2015). “Lyapunov-based Impact Time Control
664 Guidance Laws Against Stationary Targets.” *IEEE Transactions on Aerospace and Electronic*
665 *Systems*, 51(2), 1111–1122.

666 Kim, T.-H., Lee, C.-H., Jeon, I.-S., and Tahk, M.-J. (2013). “Augmented Polynomial Guidance with
667 Impact Time and Angle Constraints.” *IEEE Transactions on Aerospace and Electronic Systems*,
668 49(4), 2806–2817.

669 Kumar, S. R. and Ghose, D. (2015). “Impact Time Guidance for Large Heading Errors Using Sliding
670 Mode Control.” *IEEE Transactions on Aerospace and Electronic Systems*, 51(4), 3123–3138.

671 Lee, J. I., Jeon, I. S., and Tahk, M. J. (2007). “Guidance Law to Control Impact Time and Angle.”
672 *IEEE Transactions on Aerospace and Electronic Systems*, 43(1), 301–310.

673 Lee, S., Cho, N., and Kim, Y. (2020). “Impact-Time-Control Guidance Strategy with a Composite
674 Structure Considering the Seeker’s Field-of-View Constraint.” *Journal of Guidance, Control,*

675 *and Dynamics*, 43(8), 1566–1574.

676 Levant, A. (2001). “Universal Single-Input-Single-Output (SISO) Sliding-Mode Controllers with
677 Finite-Time Convergence.” *IEEE transactions on Automatic Control*, 46(9), 1447–1451.

678 Li, Z. and Ding, Z. (2018). “Robust Cooperative Guidance Law for Simultaneous Arrival.” *IEEE
679 Transactions on Control Systems Technology*, 27(3), 1360–1367.

680 Livermore, R. and Shima, T. (2018). “Deviated Pure-Pursuit-Based Optimal Guidance Law for
681 Imposing Intercept Time and Angle.” *Journal of Guidance, Control, and Dynamics*, 41(8),
682 1807–1814.

683 Lozier, D. W. (2003). “Nist digital library of mathematical functions.” *Annals of Mathematics and
684 Artificial Intelligence*, 38, 105–119.

685 Pearson, J. W. (2009). “Computation of hypergeometric functions.” Ph.D. thesis, University of
686 Oxford, University of Oxford.

687 Ryoo, C.-K., Cho, H., and Tahk, M.-J. (2006). “Time-to-go Weighted Optimal Guidance with
688 Impact Angle Constraints.” *IEEE Transactions on Control Systems Technology*, 14(3), 483–492.

689 Saleem, A. and Ratnoo, A. (2016). “Lyapunov-based Guidance Law for Impact Time Control and
690 Simultaneous Arrival.” *Journal of Guidance, Control, and Dynamics*, 39(1), 164–172.

691 Sang, D. K. and Tahk, M. J. (2009). “Guidance Law Switching Logic Considering the Seeker’s
692 Field-of-View Limits.” *Proceedings of the Institution of Mechanical Engineers, Part G: Journal
693 of Aerospace Engineering*, 223(8), 1049–1058.

694 Shneydor, N. A. (1998). *Missile Guidance and Pursuit: Kinematics, Dynamics and Control*.
695 Woodehead, Cambridge, UK.

696 Shtessel, Y. B., Shkolnikov, I. A., and Levant, A. (2007). “Smooth Second-Order Sliding Modes:
697 Missile Guidance Application.” *Automatica*, 43(8), 1470–1476.

698 Tahk, M. J., Shim, S. W., Hong, S. M., Choi, H. L., and Lee, C. H. (2018). “Impact Time Control
699 Based on Time-to-Go Prediction for Sea-Skimming Antiship Missiles.” *IEEE Transactions on
700 Aerospace and Electronic Systems*, 54(4), 2043–2052.

701 Tekin, R. and Erer, K. S. (2020). “Impact Time and Angle Control Against Moving Targets with

702 Look Angle Shaping.” *Journal of Guidance, Control, and Dynamics*, 43(5), 1020–1025.

703 Tekin, R., Erer, K. S., and Holzapfel, F. (2016). “Control of Impact Time with Increased Robustness
704 via Feedback Linearization.” *Journal of Guidance, Control, and Dynamics*, 39(7), 1682–1689.

705 Tekin, R., Erer, K. S., and Holzapfel, F. (2017a). “Adaptive Impact Time Control via Look-Angle
706 Shaping under Varying Velocity.” *Journal of Guidance, Control, and Dynamics*, 40(12), 3247–
707 3255.

708 Tekin, R., Erer, K. S., and Holzapfel, F. (2017b). “Polynomial Shaping of the Look Angle for
709 Impact-Time Control.” *Journal of Guidance, Control, and Dynamics*, 40(10), 2666–2671.

710 Tekin, R., Erer, K. S., and Holzapfel, F. (2018). “Impact Time Control with Generalized-Polynomial
711 Range Formulation.” *Journal of Guidance, Control, and Dynamics*, 41(5), 1190–1195.

712 Tsalik, R. and Shima, T. (2019). “Circular Impact-Time Guidance.” *Journal of Guidance, Control,
713 and Dynamics*, 42(8), 1836–1847.

714 Wang, P., Guo, Y., Ma, G., and Wie, B. (2019). “New Differential Geometric Guidance Strategies
715 for Impact-Time Control Problem.” *Journal of Guidance, Control, and Dynamics*, 42(9), 1982–
716 1992.

717 Zarchan, P. (2012). *Tactical and Strategic Missile Guidance*. American Institute of Aeronautics and
718 Astronautics, Inc., Reston, VA.

719 Zhang, S., Guo, Y., Liu, Z., Wang, S., and Hu, X. (2020). “Finite-Time Cooperative Guidance
720 Strategy for Impact Angle and Time Control.” *IEEE Transactions on Aerospace and Electronic
721 Systems*.

722 Zhang, Y., Wang, X., and Wu, H. (2014). “Impact Time Control Guidance Law with Field of View
723 Constraint.” *Aerospace Science and Technology*, 39, 361–369.

724

List of Tables

725	1	Simulation Cases of Scenario 1	35
726	2	Time-to-Go and Guidance Commands	36
727	3	Summary of Simulation Results (Scenario 2)	37
728	4	Simulation Cases of Scenario 3 and Summary of Results	38

TABLE 1. Simulation Cases of Scenario 1

Parameter	Case 1-1	Case 1-2	Case 1-3	Case 1-4	Case 1-5	Case 1-6
Shaping function	$f_1(\sigma)$	$f_1(\sigma)$	$f_1(\sigma)$	$f_2(\sigma)$	$f_2(\sigma)$	$f_2(\sigma)$
Exponent α	0.3	0.7	1	0.3	0.7	1

TABLE 2. Time-to-Go and Guidance Commands

Case	Time-to-Go	Guidance Command	Parameters
2-1	$t_{go,PPN}$	Eq. (30), with $f_1(\sigma)$ in Eq. (76)	$\alpha = 0.8, p = 8$
2-2	$t_{go,approx,small}$	$a = -\frac{K(2N-1)V^2}{r\sigma} \cos\left(\frac{\pi\sigma}{2\sigma_{lim}}\right) \text{sgn}(e_t) \left(\frac{ e_t }{ e_t(0) }\right)^\alpha$	$\alpha = 0.8, K = 8$
2-3	$t_{go,approx}$	$a = -\frac{K(2N-1)V^2}{r \sin \sigma} \cos\left(\frac{\pi}{2} \left(\frac{\sigma}{\sigma_{lim}}\right)^5\right) \text{sgn}(e_t) \left(\frac{ e_t }{ e_t(0) }\right)^\alpha$	$\alpha = 0.8, K = 8$

TABLE 3. Summary of Simulation Results (Scenario 2)

Performance Measures	Proposed	Ref. (Zhang et al. 2014)	Ref. (He et al. 2020)
Zero-effort-miss ($Z(t_f)$, [m])	$0.219 \cdot 10^{-7}$	0.016	0.022
Impact Time (t_f , [s])	55.000	55.1012	55.1352

TABLE 4. Simulation Cases of Scenario 3 and Summary of Results

Parameters and Performance Measures	Case 3-1	Case 3-2	Case 3-3	Case 3-4	Case 3-5	Case 3-6
Guidance Law	1	1	2	2	$2a$	$2a$
Desired Impact Time (s)	45	50	45	50	45	50
zero-effort-miss (m)	0.005	0.013	0.289	0.490	0.001	0.001
Time-to-Go Error ($ (t_f) - t_d , [10^{-3}s]$)	0.001	0.003	0.072	0.317	0.002	0.027
$J_{energy} [10^3 m^2/s^4]$	0.712	0.812	0.599	0.647	0.732	0.693

729

List of Figures

730	1	Engagement Geometry	40
731	2	Concept of Desired Look Angle and Reference Look Angle	41
732	3	Simulation Results for Scenario 1: Effects of Design Parameters	42
733	4	Simulation Results for Scenario 2: Comparison with Guidance Laws Based on	
734		Approximate Time-to-Go	43
735	5	Simulation Results for Scenario 3: Comparison Between Proposed Guidance Laws	44

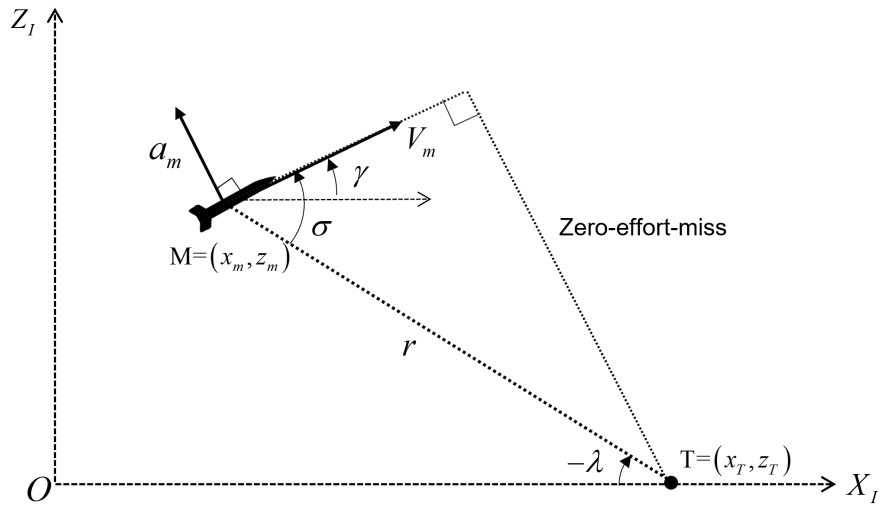


Fig. 1. Engagement Geometry

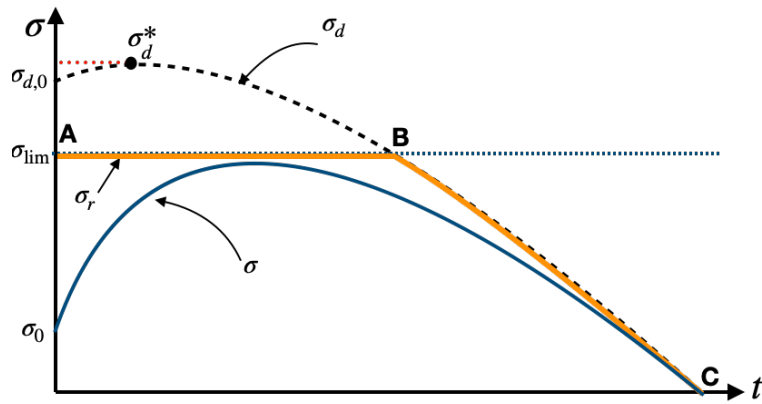


Fig. 2. Concept of Desired Look Angle and Reference Look Angle

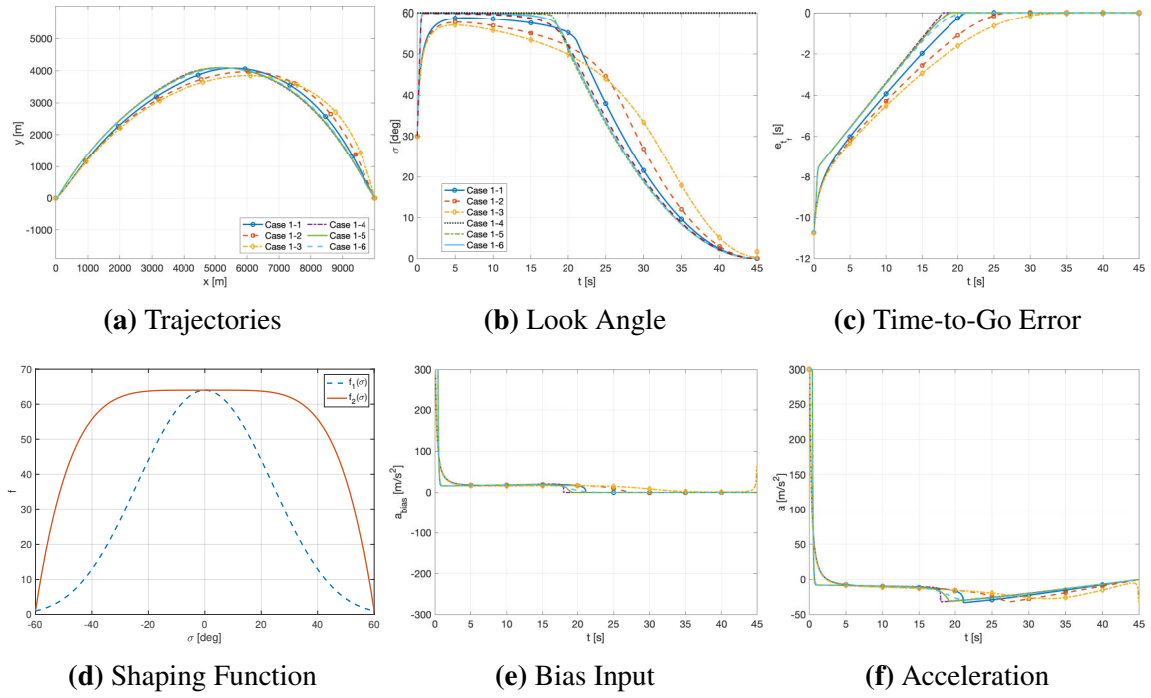


Fig. 3. Simulation Results for Scenario 1: Effects of Design Parameters

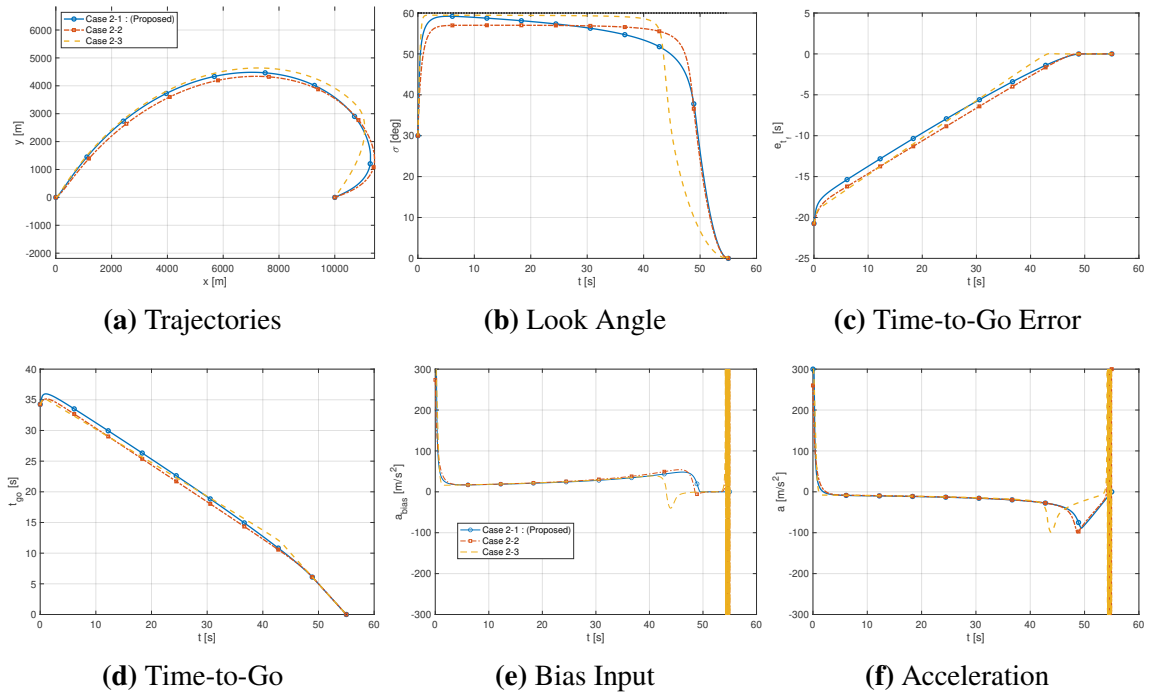


Fig. 4. Simulation Results for Scenario 2: Comparison with Guidance Laws Based on Approximate Time-to-Go

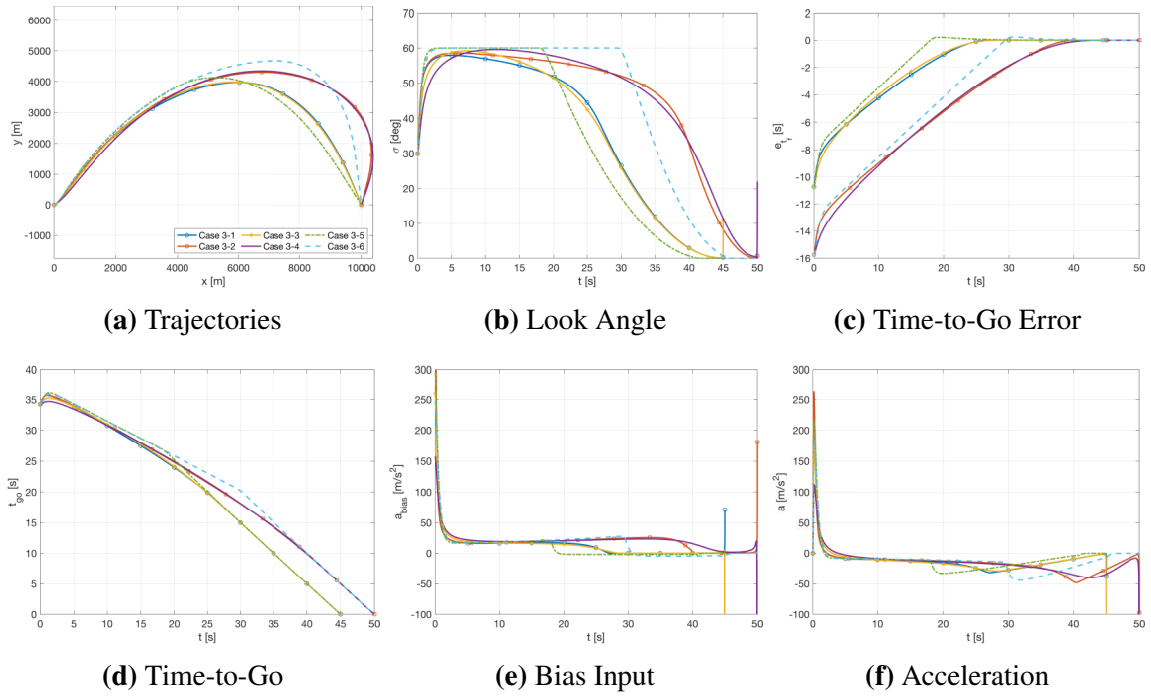


Fig. 5. Simulation Results for Scenario 3: Comparison Between Proposed Guidance Laws

2023-12-12

Analytic approach to impact time guidance with look angle constraint using exact time-to-go solution

Lee, Seokwon

American Society of Civil Engineers

Lee S, Kim J, Kim Y Cho N. (2024) Analytic approach to impact time guidance with look angle constraint using exact time-to-go solution. Volume 37, Issue 2, March 2024, Article number 5250
<https://doi.org/10.1061/JAEEZ.ASENG-5250>

Downloaded from Cranfield Library Services E-Repository